2024-08-01

Routing Optimisation for Towing a Floating Offshore Wind Turbine under Weather Constraints

Le Pivert, F

10.1016/j.oceaneng.2024.118025
Ocean Engineering
Elsevier

Ocean Engineering 305 (2024) 118025

Contents lists available at ScienceDirect

Ocean Engineering

journal homepage: www.elsevier.com/locate/oceaneng

Routing optimisation for towing a floating offshore wind turbine under weather constraints☆

Frédéric Le Pivert *, Adán López-Santander, Matthew J. Craven, Adam Roberts

Maritime Simulation Laboratory, School of Engineering, Computing and Mathematics, University of Plymouth, Plymouth, PL4 8AA, United Kingdom

ARTICLE INFO

Keywords:
Multi-objective routing optimisation
Weather routing
Genetic algorithm
Towing
Carbon emissions
Ship simulator
Floating offshore wind turbine

ABSTRACT

This paper presents a methodology for optimising routing for towing of fully assembled Floating Offshore Wind Turbines using a purpose-built ship simulator to generate datasets describing dynamics for a towing arrangement together with the engine data of the ship, and using such dataset and historical metocean data to perform multi-objective route optimisation for the tow using NSGA-II evolutionary algorithm. The work introduces the new ship simulator and the modelling of the platform VolturnUS-S, including the discussion of a comparative experiment between the model in the ship simulator and a 1:70 scale model in a wave tank. This is then followed by a presentation of the towing experiments, the characteristics of the data obtained from them, and the methodology for the optimisation of the towing routes with the following minimisation objectives: the duration of the tow, the maximum tension in the towing line, and the carbon emissions. Results are presented and discussed together with the limitations. The methodology has the potential to offer rapid and accurate results, providing a framework for safe, fast, and economical experimental process that could enhance visibility for operations before high maturity level is achieved or they can be physically performed, and contribute to improve marine operations.

1. Introduction

Major interest has been shown worldwide for offshore wind energy production. In the United Kingdom, bottom-fixed wind turbines have been extensively installed in the North Sea and other shallow sea areas, such as the Irish Sea. However, bottom-fixed technologies face challenges in areas further offshore, where wind power potential, but also water depths, are greater. This is the case in the Celtic Sea, off the west coast of England, where Leasing Round 5 of the UK Government is now targeting up to 4.5 GW of floating offshore wind capacity (The Crown Estate, 2023). Floating offshore wind platforms are therefore increasingly studied with the objective of installing offshore wind farms in these locations.

For offshore wind, marine operations —i.e. the offshore operations required for installing, maintaining, and decommissioning turbines— represent an important and significant portion of life cycle costs and carbon dioxide emissions (Castro-Santos and Diaz-Casas, 2014; Kaldellis and Apostolou, 2017). Compared to fixed bottom systems, floating devices are typically intended to operate further offshore. On top of that, floating offshore wind turbines simplify the installation process by enabling assembly in port and by introducing the possibility of more easily commissioning them at sea. When a turbine reaches the site, only a hook-up operation must be performed. This is a well-known operation in the offshore oil and gas industry, applied to the commission of oil rigs for example. In the case of floating offshore wind turbines, the hook-up operation is even simpler than for oil and gas platforms due to fewer number of connections. This work is focused on wet ocean towing of the floating wind turbine, as it is one possible way to transport them from the port to the location of the wind farm.

Nevertheless, there is currently a lack of industrial experience with deploying full-size floating turbines at scale. As a result, there are a wide range of assumptions and simplifications in many of the models that are used to inform decision making around floating wind costs and installation (Sykes et al., 2023). This highlights the importance of the development of new technologies and tools for the simulation of marine operations, not only in view of decreasing costs and environmental impact, but also aiding developers reduce the uncertainty within project plans.

☆ This document is an output of the *Cornwall Flow Accelerator* project, part funded by the European Regional Development Fund for Cornwall, project number: O5R19P03188.

* Corresponding author.
E-mail addresses: frederic.lepivert@plymouth.ac.uk (F. Le Pivert), adan.lopez-santander@plymouth.ac.uk (A. López-Santander), matthew.craven@plymouth.ac.uk (M.J. Craven), adam.roberts@plymouth.ac.uk (A. Roberts).

https://doi.org/10.1016/j.oceaneng.2024.118025
Received 6 March 2024; Received in revised form 15 April 2024; Accepted 24 April 2024
Available online 2 May 2024

This paper introduces a new maritime ship simulator in the Maritime Simulation Laboratory at Plymouth University. This tool can be used to investigate the costs and environmental impact of offshore operations for floating offshore wind energy, and here it is used to examine the ocean transportation of a floating offshore wind turbine. A ship simulator can be advantageous for this application, as it facilitates straightforward modelling of the behaviour of the towing ship, floating offshore wind turbine, and towing line. The accuracy of the simulated behaviours depends entirely on the accuracy of the data that was used to define the properties of the different objects in the model. There already exists literature discussing floating offshore wind turbine motions under different sea conditions, see for instance Leimeister et al. (2018), and Liu and Yu (2022). Consequently, the ability of the new simulator to reproduce the motions of a floating offshore wind turbine when moored is also discussed for the purpose of model verification.

The paper also focuses on a methodology for the multi-objective optimisation of ocean towing routes using simulator generated data and evolutionary algorithms. Results from experiments run with the Maritime Simulation Laboratory's ship simulator have been used to generate an empirical model of a single ship towing a floating offshore wind turbine in oceanic conditions — i.e. deep waters that are well away from other marine traffic and features such as river mouths and port structures. This model describes three quantities as functions of true wind speed, wind angle, and towing vessel's engine order:

1. power of each engine of the towing ship;
2. tension in the towing line;
3. surge velocity.

One type of platform is considered in this work, however many different designs of floating offshore wind turbines exist, and the dynamics of some of them when towed have already been studied (Myland et al., 2014; Le et al., 2021). The UMaine VolturnUS-S Reference Platform, developed for the IEA Wind 15-Megawatt offshore reference wind turbine (Gaertner et al., 2020; Allen et al., 2020), hereafter referred to as *VolturnUS*, is larger than the wind turbines studied before and is used in this paper. Its response over swell has been studied with decay tests and in moored conditions (Holcombe et al., 2023), providing data used for verifying the ship simulator implementation of this turbine.

The physical problem of wet towing has previously been discussed and considered for several types of towed platforms. For instance, Amin et al. (2021) considered the seakeeping of a towed floating desalinisation plant, and Zhu and Hu (2021), Park et al. (2021) performs a unified seakeeping and manoeuvring analysis for different kinds of tow. Also, optimisation of ship routing has been extensively discussed using different approaches. This subject has often been motivated by the effect that weather has in shipping, ultimately aiming to avoid severe weather conditions, and by pursuing several objectives: energy efficiency, ship safety, or reducing the duration of the voyage. For examples, see James (1957) for an early work using isochrones, Gershanik (2011), Shao et al. (2012), and Lin et al. (2013) for approaches using dynamic programming, Chauveau et al. (2017) and Grifoll et al. (2022) for shortest path techniques, Szlapczynska and Smierzchalski (2007) using isochrones and evolutionary algorithms, or Walther et al. (2016) and Wang et al. (2017) for comparative studies.

The family of genetic algorithms has already been proposed for solving the problem of ships' weather routing as already seen in Szlapczynska and Smierzchalski (2007). Furthermore, Kuhlemann and Tierney (2020) proposes the use of evolutionary algorithms to optimise fuel consumption considering wind and waves and Kim and Kim (2017a) propose the use of such algorithms for ocean towing of offshore structures.

A variety of genetic algorithms have been developed (Konak et al., 2006) to solve different problems, e.g. Jiao et al. (2017) and Gai et al. (2017). Among multi-objective genetic algorithms, NSGA-II —the non-dominated sorting genetic algorithm (Deb et al., 2002)— is a fast and elitist genetic algorithm, adapted to multi-objective optimisation, which is used in the present work. At the end of an algorithm run, a set of routes is obtained — named the Pareto front approximation. Every route of this approximation is an optimum estimate for that algorithm run according to the objective functions used, and forms a trade-off between the objectives. Decision makers could then use some criterion to choose the most suitable route from the Pareto front approximation. Due to the real-world nature of the problem the true Pareto front is unknown. For the problem of ship routing, an accurate and efficient prediction of ship behaviour in different conditions is needed (Vettor and Guedes Soares, 2022; Kuroda and Sugimoto, 2022) and used as input to genetic algorithms.

Several authors have previously explored single-objective ship route optimisation using different methods. For example, Du et al. (2021) look at how adjusting engine power according to the weather conditions influence the optimal choice from three predetermined routes for an oil tanker travelling across the Atlantic. The focus was on minimising either estimated time of arrival, or fuel consumption and carbon emissions. A similar transatlantic voyage has been examined (Du et al., 2022) using a three-dimensional – latitude, longitude, and time – dynamic programming algorithm. For this, navigational way points are generated alongside an initial reference route, which the ship can turn towards provided certain criteria are met. This was combined with single-objective optimisation to minimise either fuel usage – and hence emissions and costs – or voyage time under given weather conditions. Another example is Vettor et al. (2021), who optimised the navigational risk – here defined as a seakeeping response exceeding an acceptable value – and evaluated the associated performance: mean and variance of the fuel consumption and voyage time. This ultimately enables route ranking and thus minimisation of either of these quantities. Further examples include Zaccone et al. (2018), who used single-objective optimisation in conjunction with a dynamic programming algorithm to minimise fuel consumption, and Kim and Kim (2017b), who examined a tug towing a platform and used genetic algorithms to conduct single-objective optimisation to independently minimise travel distance, travel time, or towline tension for routes between Rongcheng, China and Jeju Island, Korea.

Multi-objective weather routing optimisations – i.e. optimising for multiple objectives simultaneously – have also been performed, considering transatlantic or Western Mediterranean voyages. A three-objectives optimisation using Martins algorithm (Martins, 1984) has been presented by Fabbri and Vicen-Bueno (2019). The objectives considered are minimising voyage time, wave added resistance and loss of stability on swell. Multi-objective evolutionary algorithms have also been used to perform weather routing optimisations, such as in Krata and Szlapczynska (2018) and Szlapczynska and Szlapczynski (2019) where the objectives are minimising the passage time, fuel consumption and increasing safety of passage. The role of the evaluation of the amplitude of the ship roll motion is measured in Krata and Szlapczynska (2018). The use of preference-based multi-objective evolutionary algorithm is discussed in Szlapczynska and Szlapczynski (2019). The role of such algorithm is to reduce the size of the Pareto front.

Furthermore, a multi-objective evolutionary algorithm has also been explored to optimise routing in real-time (Vettor et al., 2020). Such optimisation is implemented in a real-time software that considers simultaneously the following three objectives:

- minimising fuel consumption;
- minimising passage time;
- minimising risks by sailing.

The present paper adds to the literature by proposing routing optimisations considering the towing dynamics between a vessel and towed floating offshore wind turbine. Both single objective and multi-objective evolutionary algorithms have been applied to the objectives of minimising transport duration, minimising carbon emissions, and minimising towline tension. These algorithms are ultimately used to generate optimised routes between the Bill of Portland, and a site in the

Fig. 1. Bridge of the ship simulator.

Celtic Sea, without the need for a predefined reference path or spatial way points. To do this, a model to compute the tension in the towing line, the power delivered by the engines of the towing ship, and the surge velocity of the tow has been derived from series of simulations run in a new ship simulator built for this purpose. The model considers the complex dynamics of multi-object interactions.

2. Materials

2.1. Ship simulator

The ship simulator has been commissioned and built by the Maritime Simulation Laboratory of the University of Plymouth in collaboration with Kongsberg Digital. This tool permits rapid experimentation in a safe, virtual environment, enabling efficient investigation of how metocean conditions and operational parameters influence timescales, economics, and environmental costs. Unlike traditional numerical methods — such as computational fluid dynamics, the physics engine of the simulator does not use general laws, e.g. the Navier–Stokes equations, to directly model fluid–structure interaction. Instead, hydrostatic and hydrodynamic forces are accounted for using algebraic expressions that rely on empirical coefficients. This provides the advantage of rapid simulation of multiple objects, and by extension, rapid generation of data that can be used to aid decision-making. A drawback of this approach is that it relies on the availability of sufficient accurate input data for each object; for example, hydrodynamic drag coefficients as a function of Reynolds number and flow angle. This data must come from either practical experimentation or higher fidelity numerical models that have ideally undergone appropriate verification and validation.

The simulator is composed of several components:

- a bridge simulator, K-Sim Navigation, that received from DNV-GL a statement of compliance with class A - Standard DNVGL-ST-0033 for certification of Maritime Simulators (DNV-GL DET NORSKE VERITAS, 2017); see Fig. 1, consoles of the middle and on the right;
- a dynamic positioning simulator, K-Sim Dynamic Positioning, that received from DNV-GL a statement of compliance with class A - Standard DNVGL-ST-0033 for certification of Maritime Simulators (DNV-GL DET NORSKE VERITAS, 2017); see Fig. 1, two consoles on the left;
- an instructor station to create scenarios for the simulation;
- a design station to model vessels, define hydrostatics and dynamics, define the position, the characteristics and, if needed, the dynamics of different parts such as thrusters, engines, or rudders.

Table 1
Notations.

Symbol	Denotes
ρ	Density of seawater
ρ_A	Density of air
A	Wetted area of the hull
A_A	Area exposed to wind of the whole structure
U	Horizontal speed
w	Heave velocity
p	Roll velocity
q	Pitch velocity
r	Yaw velocity
r^*	Adimensionalised rate of turn
ν	Kinematic viscosity
L	Length of hull
LOA	Length over all
B	Beam (width) of hull
T	Draught of hull
m or Δ	Displacement of floating body
GM	Metacentric height
g	Gravity acceleration
C_{WP}	Waterplane area coefficient
I_{xx}	Moment of inertia around x-axis
I_{yy}	Moment of inertia around y-axis
∇_0	Nominal buoyancy volume
∇_1	Actual submerged volume
V_{WR}	Apparent wind speed
z_A	Height of the centre of aerodynamic effort
$C^{(0,1,2)}_{Y,N,Z,K,M}$	Various model coefficients
K	Moment around the x-axis
M	Moment around the y-axis
N	Moment around the z-axis
X	Force along the x-axis
Y	Force along the y-axis
Z	Force along the z-axis
BP	Bollard Pull

The ship simulator is also able to interface with other software via an Application Programme Interface (API) implemented by Kongsberg Digital. It streams data at two different rates depending on the variable: 30 Hz and 2 Hz. It is also possible for the user to send commands and change parameters' values via the same API. In the present paper, this has been used to control the course of the ship.

In the ship simulator, the dynamics of the bodies are computed by solving the fundamental principle of the dynamics. The forces and moments applied to a body are described by Eqs. (1)–(3) and (5)–(7), all of them defined by Kongsberg Digital. All the notations used in this section are listed in Table 1.

The resistance of a floating object is defined by

$$X = \frac{\rho A}{2}\sqrt{U^2 + r^2L^2}C_X^{(0)}\left(\sqrt{U^2 + r^2L^2}C_X^{(1)} + \frac{\nu}{T}C_X^{(2)}\right), \tag{1}$$

where

$C_X^{(0)}$ is a drag coefficient depending on rate of turn, drift, relative water depth, roll and pitch angles, and relative heave position;
$C_X^{(1)}$ translates the hull wave resistance;
$C_X^{(2)}$ translates the viscous and turbulent resistance.

The manoeuvrability efforts are described by

$$\begin{aligned} Y &= \frac{\rho A}{2}(U^2 + r^2L^2)C_Y^{(0)}C_Y^{(1)}C_Y^{(2)}, \\ N &= \frac{\rho A}{2}L(U^2 + r^2L^2)C_N^{(0)}C_N^{(1)}C_N^{(2)}, \end{aligned} \tag{2}$$

where

$C_Y^{(0)}$, $C_N^{(0)}$ are the manoeuvring coefficients depending on rate of turn, drift and relative water depth;
$C_Y^{(1)}$, $C_N^{(1)}$ translate the dependence of the manoeuvring efforts on the Froude number;
$C_Y^{(2)}$, $C_N^{(2)}$ translate the dependence of the manoeuvring efforts on roll and pitch angles, and relative heave position.

The hydrodynamics of the other degrees of freedom are defined by the set of equations

$$\begin{aligned} Z &= \frac{\rho A}{2}\left(-w\left(C^{(Z)}C_Z^{(0)} + |w|C_Z^{(1)}\right) + U^2 C_Z^{(2)}\right) \\ K &= \frac{\rho A}{2}B\left(-p\left(C^{(K)}C_K^{(0)} + |p|C_K^{(1)}\right) + U^2 C_K^{(2)}\right) \\ M &= \frac{\rho A}{2}L\left(-q\left(C^{(M)}C_M^{(0)} + |q|C_M^{(1)}\right) + U^2 C_M^{(2)}\right) \end{aligned} \tag{3}$$

where

$C_Z^{(0)}$, $C_K^{(0)}$, $C_M^{(0)}$ are the linear damping coefficients depending on Froude number;
$C_Z^{(1)}$, $C_K^{(1)}$, $C_M^{(1)}$ are the quadratic coefficients depending on Froude number;
$C_Z^{(2)}$, $C_K^{(2)}$, $C_M^{(2)}$ are correction coefficients depending on relative depth, drift, Froude and Froude displacement numbers, roll and pitch angle, and relative heave position.

And the parameters $C^{(Z)}$, $C^{(K)}$, $C^{(M)}$ are defined by the set of equations

$$\begin{aligned} C^{(Z)} &= \frac{1}{2\pi}\sqrt{gC_{WP}LB\nabla_0^{-\frac{1}{3}}} \\ C^{(K)} &= \frac{1}{2\pi}\sqrt{\frac{gmB}{I_{xx}}} \\ C^{(M)} &= \frac{1}{2\pi}\sqrt{\frac{gmL}{I_{yy}}}. \end{aligned} \tag{4}$$

The aerodynamic efforts are represented as follows

$$\begin{aligned} X_A &= \frac{1}{2}\rho_A A_A V_{WR} C_{AX} \\ Y_A &= \frac{1}{2}\rho_A A_A V_{WR} C_{AY} \\ N_A &= \frac{1}{2}\rho_A A_A . L V_{WR} C_{AN}, \end{aligned} \tag{5}$$

where C_{AX}, C_{AY} and C_{AN} are functions of the apparent wind angle. Moreover, an aerodynamic heeling moment is being calculated using the equation

$$K_A = z_A . Y_A. \tag{6}$$

The hull hydrostatics are calculated with the equation

$$F_{hydrostatic} = \rho g \nabla_1. \tag{7}$$

The hydrostatic force is applied from the centre of buoyancy of the body. If the vessel has a standard hull shape (namely a ship), it is possible to define the restoring arm as a function of the roll angle and therefore the ship simulator computes a nonlinear hydrostatic restoring moment. The ship simulator computes wave effects, blank effects, and ship-to-ship interactions. However, these have not been taken into account in the present paper.

The towing lines, or any line, are assumed to be flexible. The tension is calculated by solving the fundamental principle of the dynamics along the lines. The tension at the line ends are outputs of the simulator's API streams and can be read by the user in real-time. Different line's materials and diameters can be used and the choice will affect the calculations.

The environment within the simulated world is controllable, with currents, wind, and waves being definable by the user. These can be defined as global variables, meaning they are the default values for the entire simulated world and apply everywhere — unless specified otherwise by using localised variables that are mapped to user-defined spatial regions.

The waves can be generated by default as a result of the wind or by defining a profile. In the earlier case, the development of the sea state can be set and the waves will come from the same direction as the wind on average. The bathymetry of the area is defined by the nautical chart in use. If a simulated object is located beyond the nautical chart limits, then a water depth can be defined by the user.

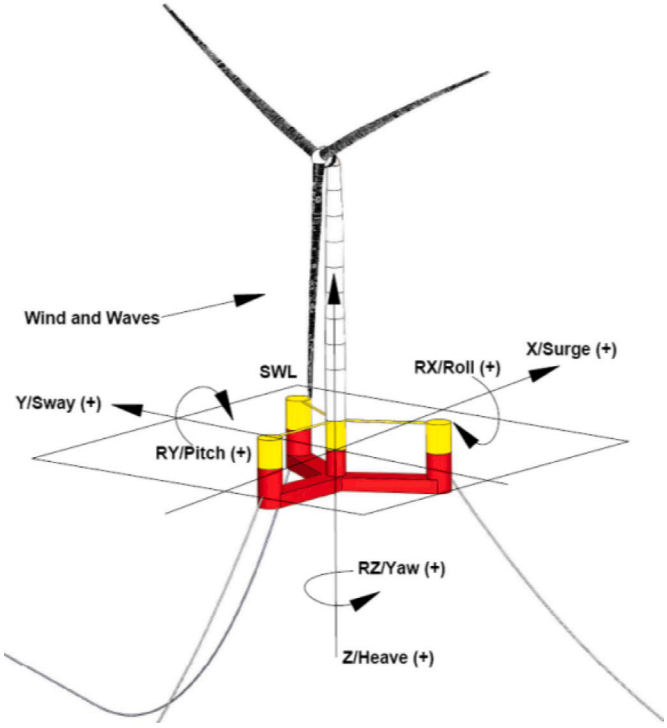

Fig. 2. VolturnUS with axis definition, picture provided by NREL (Allen et al., 2020).

Table 2
Characteristics of the floating wind turbine (Allen et al., 2020).

Characteristics	Value
LOA (m)	90.1
B (m)	102.1
T (m)	19.12 (aft), 19 (fore)
Freeboard (m)	15
Δ (t)	20 090
GM (m)	25.67 (longitudinal), 25.81 (transversal)

2.2. Floating wind turbine

The floating offshore wind turbine considered is the full-scale *VolturnUS* (Allen et al., 2020), as summarised in Fig. 2 and Table 2 for the axes definition and the main characteristics respectively. The development of the *VolturnUS*'s simulator model was done by the authors of this study, and the turbine is assumed to be fully ballasted in all cases, including calculations of hydrostatics and inertia. This was driven by data availability, both in terms of creating the digital model of the *VolturnUS* and in particular for having experimental data to verify behaviour against, however it must be noted that floating offshore wind turbines are typically towed in a deballasted condition. This limitation is deemed acceptable given that the aim of this paper is not to optimise the towing configuration specifically, but to instead introduce a methodology for using a ship simulator within multi-objective route optimisation of towing operations.

The matrix of hydrostatic stiffness, described in Eq. (8), has been computed using the design capabilities as designed by Kongsberg Digital:

$$C = \begin{pmatrix} 0 & 0 & 0 & 0 & 0 & 0 \\ 0 & 0 & 0 & 0 & 0 & 0 \\ 0 & 0 & 4.379E6 & 4.379E6 & 0 & 0 \\ 0 & 0 & 4.379E6 & 2.495E8 & 0 & 0 \\ 0 & 0 & 0 & 0 & 1.789E8 & 0 \\ 0 & 0 & 0 & 0 & 0 & 0 \end{pmatrix}, \tag{8}$$

where the units are N/m, N/rad and Nm/rad.

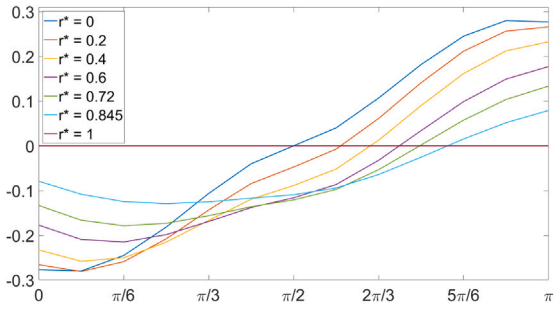

Fig. 3. Drag coefficients of the *VolturnUS* as a function of the drift angle.

Fig. 4. Picture of the AHTS Normand Ranger, provided by Solstad Offshore (2023).

Table 3
Characteristics of the towing vessel.

Characteristics	Value
LOA (m)	91
B (m)	22
T (m)	7.98 (aft), 8.02 (fore)
BP (t)	280
Propulsion equipment	2 pitch-controllable propellers
Engines	4 diesel engines
Other generators	2 speed shaft generators (PTO/PTI)
Steering equipment	2 rudders

Table 4
Specifications of seakeeping experiment.

Positions of nodes				
ID	X (m)	Y (m)	Z (m)	Object
1	−58	0	−14	Vessel
2	29	50.229	−14	Vessel
3	29	−50.229	−14	Vessel
4	−480	0	−70	Seabed
5	240	415.692	−70	Seabed
6	240	−415.692	−70	Seabed
Connections				
L (m)	Seabed node	Vessel node		
450.6	4	1		
450.6	5	2		
450.6	6	3		
Sea states				
Origin	H_S (m)	T_P (s)	γ	Thrust (N)
$-x$	1.8	9.1	1	1 982 540
$-x$	5.5	9.0	5	1 982 540

The matrix of inertia and the added mass matrix used in this work are the same as in Allen et al. (2020) and the aerodynamic coefficient has been computed for a fully feathered turbine, i.e. considering the turbine minimising its drag and, hence, it is assumed that the aerodynamic forces are minimal regardless of the direction of the wind. Furthermore, the vertical aerodynamic moment is not considered for this study. The other hydrodynamic coefficients have been modelled assuming a box shaped hull hydrodynamic model. The drag coefficient $C_X^{(0)}$ is represented in Fig. 3 for different adimensionalised rates of turn $r^* = \frac{rL}{\sqrt{(rl)^2 + U^2}}$.

2.3. Towing ship

The towing ship used in the experiments is a digital model of Normand Ranger (Fig. 4). Normand Ranger is an Anchor Handling and Tug Supply (AHTS) vessel built in 2010 by Ulstein Verft (Ulstein, 2010) in collaboration with Solstad Offshore (Solstad, 2010). This vessel was selected as it is the most powerful tug currently available in the ship simulator, ensuring that it would be capable of successfully completing as many towing simulation runs as possible regardless of metocean conditions, and thus generate the most data for optimisation. The characteristics of the ship are provided in Table 3. The model has been implemented by Kongsberg Digital and it is referred to as *Defender*. Kongsberg Digital implements the simulator's digital ship models based on extensive testing, verification, and validation processes, but are unable to provide the source files due to commercial constraints.

3. Methodology

3.1. Comparison of experiments from a wave tank and in the simulator

The University of Plymouth has previously conducted experiments in the COAST Laboratory's wave tank to measure the seakeeping of a 1:70 scale model *VolturnUS* that is moored in Celtic Sea conditions for a separate study (Tosdevin et al., 2023). The sea states were representative of those that have been observed for the Celtic Sea and the scaled water depth for the experiments was equivalent to 70 m of real water depth. The specifications of the experiment are summarised in Table 4, with all specifications and results described here rescaled to full-scale. Further details of experimental procedure can be found in Tosdevin et al. (2023). The thrust is a force applied to the *VolturnUS* nacelle to represent the aerodynamic load due to the wind. Information about the scale model of the *VolturnUS* can be found within the first FOWT comparative study dataset (Ransley et al., 2022).

The results of these experiments were shared to conduct a comparison against the simulated turbine. Although (Tosdevin et al., 2023) was not a towing experiment, it was decided to replicate the study at full-scale within the ship simulator in order to verify whether the digital model of the *VolturnUS* has been implemented reliably due to the availability of data for appropriate metocean conditions. This will not fully validate the towing portion of the study, but will provide initial confidence that the *VolturnUS* responds in an appropriate fashion to the simulated metocean conditions. The following factors and differences between the practical test and simulator should be noted:

- wind effects have not been considered in either experiment;
- the waves produced by the simulator are not unidirectional and have components in different directions (see Figs. 5 and 6);
- the forces applied to the *VolturnUS* are calculated using wamit files with extensions .1, .3, .4 and .9 (WAMIT, 2011) and the matrix of viscous drag coefficients;
- the viscous drag coefficients come either from Holcombe et al. (2023) or from Allen et al. (2020) if they were not evaluated previously;
- the hydrodynamic model considered for the optimisation was not considered in the validation experiment.

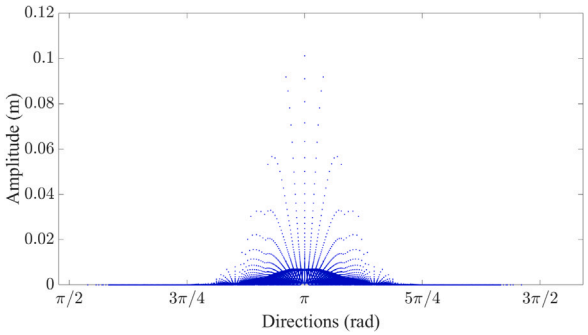

Fig. 5. Amplitudes against directions of the waves components of the first sea state.

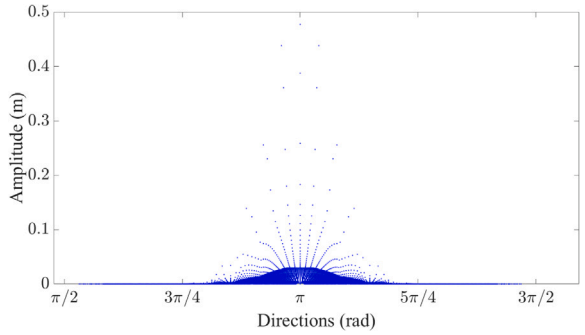

Fig. 6. Amplitudes against directions of the waves components of the second sea state.

3.2. Towing simulations

In the simulations, the *VolturnUS* turbine is towed from the stern by the AHTS *Defender*. The towing arrangement (Fig. 7) is inspired by the example of Dagher et al. (2017), with the platform is towed with a connection from a single column. It should be noted, however, that there are shape differences between the rectangular hull scale model tested by Dagher et al. (2017), and the cylindrical hulls of the full scale *VolturnUS*. These shape and size differences could render this configuration less practical or effective for a real full-scale platform, however it is assumed to be acceptable for the purposes of this work. It is composed of the following:

- a tow briddle plate;
- a steel wire 144 mm diameter line of a paid out length of 1167.7 m between the *Defender* and the tow bridle plate;
- a steel wire 77 mm diameter line of a length of 101.3 m connecting the tow briddle plate and the *VolturnUS*, moored on starboard;
- a steel wire 77 mm diameter line of a length of 101.4 m connecting the tow briddle plate and the *VolturnUS*, moored on port.

Since the focus of this paper is only on the oceanic portion of towing – and does not consider manoeuvring in ports, or in places that require greater control such as near river mouths – only a single towing vessel is used. Tow integrity has not been considered in the routing optimisation and the towing arrangement of the experiments in the simulator is over-dimensioned, for it is not the intention for such arrangement to represent a real towing plan, but to provide an experimental platform capable to be run in a broad range of weather conditions, including extreme winds, without failing. Hence, the oversized dimension of the cables used and simulation of wind speeds of up to 60 knots, which is likely to be too severe for real-world towing but of interest to include during the optimisation. The connection points, where the towing lines are fixed on the *VolturnUS*, are aligned with the centre of gravity of the platform.

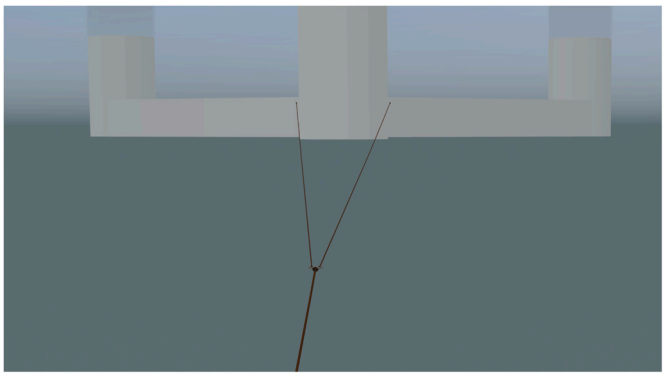

Fig. 7. Towing arrangement.

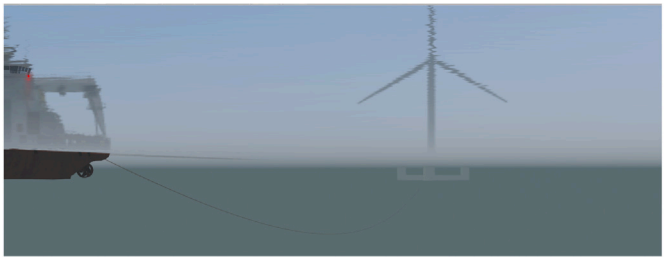

Fig. 8. Simulated towing operation seen from port to *Defender* and underwater.

Table 5
Completed experiments.

Throttles			
Wind speed (knots)	0.5	0.75	1
0	No	No	Yes
5	Yes	Yes	Yes
10	Yes	Yes	Yes
15	Yes	Yes	Yes
20	Yes	Yes	Yes
25	Yes	Yes	Yes
30	Yes	Yes	Yes
35	Yes	Yes	Yes
40	Yes	Yes	Yes
45	Yes	Yes	Yes
50	No	Yes	Yes
55	No	No	Yes
60	No	No	Yes

A picture of the simulated towing operation in calm sea is provided in Fig. 8.

While running the towing experiments, the course is maintained by the autopilot and the engine order for the *Defender* is set to be one of 0.5, 0.75, or 1 of its maximum value. The wind direction is from the North and the waves are generated by the wind, with sea development set to be maximal, i.e. fully developed.

For each experiment, the course of the autopilot changes from 0° to 180° in steps of 30° throughout the simulation. The experiment will maintain the course set by the autopilot for five minutes during each step once the tow has stabilised within ± 3° of the required course for at least 30 s. If this is not achievable, the experiment will be cancelled and the data disregarded.

In Table 5 all experiments that could be completed and for which data exist are listed. The data collected are in the form of time series. The list of collected data is given in Table 6.

Table 6
Collected data.

Object	Data	Description
Defender	Position	3 dimensions
	Attitude	3 angles
	Linear velocity	Along 3 axes
	Rotational velocity	Around 3 axes
	Hydrodynamic force	Along 3 axes
	Hydrodynamic moment	Around 3 axes
	Wave force	Along 3 axes
	Wave moment	Around 3 axes
	Aerodynamic force	Along 3 axes
	Aerodynamic moment	Around 3 axes
	Rudder angle	2 rudders
	Course through water	
VolturnUS	Position	3 dimensions
	Attitude	3 angles
	Linear velocity	Along 3 axes
	Rotational velocity	Around 3 axes
	Hydrodynamic force	Along 3 axes
	Hydrodynamic moment	Around 3 axes
	Wave force	Along 3 axes
	Wave moment	Around 3 axes
	Aerodynamic force	Along 3 axes
	Aerodynamic moment	Around 3 axes
	Course through water	
VolturnUS Connection Points	Line tension	1 per connection point
	Line direction	1 per connection point
	Line elevation	1 per connection point
Autopilot	Course order	1 angle
Engines	Fuel consumption rate	1 per engine
	Torque	1 per engine
	Power	1 per engine
AHW	Speed order	
	Line tension	
Wind	Direction	True
	Speed	True

3.3. Creation of models

For every engine order, models have been created considering the power of the engines, the tension in the towing line, and the surge velocity of the *VolturnUS* as functions of true wind angle and true wind speed.

There are four diesel engines on the *Defender*. Among them, two engines are Wärtsilä 16V32 producing 8 MW at 750 RPM and the two other are Caterpilar 3516C producing 2.1 MW. In this paper, they are respectively named the main and auxiliary engines and are referred to in equations using the indices *main* and *aux* followed by a location statement in case they need to be differentiated. There are also two electric engines referred to as PTI and in equations using the index PTI followed by a location statement in case they need to be differentiated. A model of power $\mathcal{P}$ is created for each type of engine.

The model for the power of the main engines is calculated with the equation

$$\mathcal{P}_{main} = \overline{\mathcal{P}_{main\_port} + \mathcal{P}_{main\_starboard}} \tag{9}$$

where $\overline{VA}$ denotes the mean of the random variable VA.

The model for the power of the auxiliary engines is calculated with the equation

$$\mathcal{P}_{aux} = \overline{\mathcal{P}_{aux\_port} + \mathcal{P}_{aux\_starboard}}. \tag{10}$$

The model for the power of PTI engines is calculated by

$$\mathcal{P}_{PTI} = \overline{\mathcal{P}_{PTI\_port} + \mathcal{P}_{PTI\_starboard}}. \tag{11}$$

The model for the tension T in the towing line is calculated using the tension measured at the connection points of the *VolturnUS*

$$T = \overline{T_{port} + T_{starboard}} + 5\sigma\left(T_{port} + T_{starboard}\right), \tag{12}$$

where $\sigma(VA)$ denotes the standard deviation of the random variable VA.

The model for the surge velocity U is calculated by averaging surge velocity.

Following the calculations described in Eqs. (9), (10), (11), (12) the models are 2D-arrays with entries that are the true wind speeds and true wind angles used in the simulations.

Any missing values in the arrays are calculated by interpolation using functions from the Python subpackage `scipy.interpolate`: `griddata` with a cubic method or `Rbf` in case the preceding method was not applicable (Virtanen et al., 2020).

The speed predicted for the *VolturnUS* towed by *Defender* ranges between a maximum of 3.21 m/s at an engine order of 1 when sailing downwind with a wind speed of 60 knots — i.e. with a 60 knot tailwind — and a minimum of 1.11 m/s at an engine order of 0.5 when sailing upwind with a true wind angle of 30° and a wind speed of 40 knots.

3.4. Navigation

The route starts from the Bill of Portland (latitude: 50.4° North, longitude: 2.5° West) and has a goal to an arrival point in the Celtic Sea (latitude: 49.1° North, longitude: 8.5° West). The route is considered to be completed once the *VolturnUS* is within a range of 3 km of the arrival position.

The date chosen for the start is 1st August 2020, 2021, and 2022. The route starts between midnight and noon. The weather data used has been extracted from the ERA5 dataset (Hersbach et al., 2023) using the variables "10 m u-component of wind" and "10 m v-component of wind" to represent the wind. The tidal currents data comes from Copernicus® (E.U. Copernicus Marine Service Information, 2024) and every multi-objective optimisation has been run with and without considering tidal currents. Geostrophic currents are not considered in this paper. The work uses OceanWise bathymetry data published by Digimap® (OceanWise, 2023). The minimum depth threshold for safe navigation towing the *VolturnUS* has been set at 40 m and the routing is considered as having failed whenever it enters this depth contour.

During the computation of the route, a new position and metrics are calculated every minute and at each time step, a new surge velocity, towing line tension, and engine power are interpolated from the models using the function `RectBivariateSpline` from the python subpackage `scipy.interpolate` (Virtanen et al., 2020). However, the course and the engine order are changed every hour.

Hence, the new position is computed by integration of the velocity over time and the energy used by the engines is computed by integration of the power over time.

3.5. Genetic algorithms

Genetic algorithms are part of the class of evolutionary algorithms, which seek to optimise some objective function(s) given a problem and its representation. As such, the algorithm operations are modelled on Darwinian principles of natural evolution. In brief, an initial population of, often random, solutions – *genomes*, which can be represented by binary strings, vectors of real numbers or in other ways – is produced. These are then ranked according to the objective function(s), after which operations of selection, crossover and mutation, often depending upon the objective values, are used to produced the next population. Crossover is an operation that takes two or more solutions and combines them to produce one or more children for the next population — this typically results in solutions notably distinct from their parents while retaining the 'building blocks' of effective solutions. Mutation typically acts on one solution and modifies it in some small way to produce a child for the next population which is similar to its parent. This process is continued until some termination condition is invoked; such conditions include running to some specified time budget, or a given number of populations being produced.

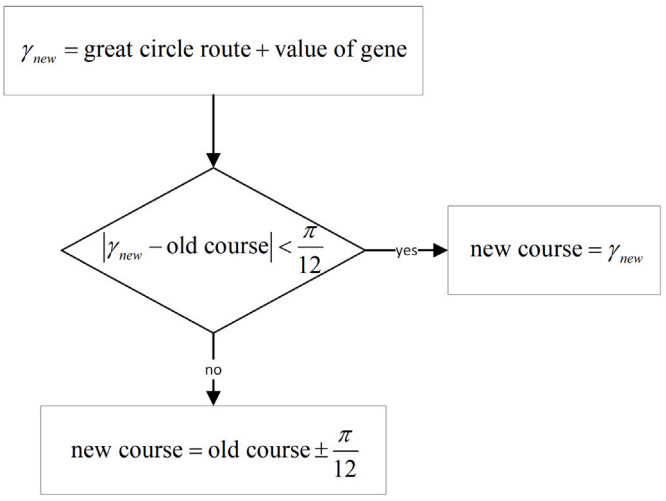

Fig. 9. Diagram for the calculation of the course.

Table 7
Parameters of the genetic algorithms.

Parameter	Value
Length of genome	401
Number of generations	4 & 100
Population	32
Multi-objective algorithm	`NSGA-II`
Single-objective algorithm	`MixedVariableGA`

As mentioned previously, the multi-objective algorithm NSGA-II is used in this work. This algorithm retains the same essence of the above, but uses non-dominated sorting to produce better solutions. Non-dominated sorting (Deb et al., 2002) allows the algorithm to say whether one solution is better than another according to several objectives. Ties in solution quality are solved by using crowding distance. Broadly, crowding distance measures the Euclidean distance between a solution and its nearest neighbour either side in the objective space. Solutions with higher crowding distance, meaning that the solutions are more widely spread, and so cover more of the objective trade-off, are preferred.

There are three kinds of genes in the genome which represent important aspects of the route:

1. genes that affect the course of the *Defender* and the *VolturnUS* – the values of these genes are angles and their values are in the interval $\left[-\frac{\pi}{8}, \frac{\pi}{8}\right]$ rad, i.e., $\pm 22.5°$;
2. genes that indicate the engine order – the values of these genes are either 0.5 or 0.75 or 1;
3. one gene that indicates the time in hour for the start – the value of this gene is an integer between 0 and 12.

The course of the *Defender* and the *VolturnUS* is calculated as in the diagram of Fig. 9.

The genetic algorithms come from the Python library `pymoo` (Blank and Deb, 2020). In this paper, the authors have only looked for solutions by modifying the parameters in Table 7. To run the algorithms, the language is Python 3.11 and the library used to read grib files is `eccodes` (European Centre for Medium-Range Weather Forecasts (ECMWF), 2005).

The other parameter values of crossover, mutation, and so on are set to the default values given by the `pymoo` library. For the multi-objective optimisation, three objectives and one constraint are considered. The objectives are:

- minimising the duration of the transportation;
- minimising the maximum tension in the towing line;
- minimising the carbon emissions.

Table 8
Weights for the cost function in single-objective optimisations.

Objective	Weight O99	Weight O90
Duration	1	1
Tension	0.05	0.05
Carbon emissions	0.1	0.01

Table 9
Comparison of results for the first sea state.

Quantity	Wave tank	Simulator
$\overline{\theta}$	8.06E−2 rad	5.00E−2 rad
$\sigma(\theta)$	2.07E−3 rad	4.12E−3 rad
$\overline{\phi}$	6.34E−3 rad	−3.20E−9 rad
$\overline{\psi}$	2.35E−2 rad	−1.08E−4 rad
Line tension 1	2.34E6 N	2.48E6 N
Line tension 2	4.62E5 N	4.69E5 N
Line tension 3	1.51E5 N	4.69E5 N

Table 10
Comparison of results for the second sea state.

Quantity	Wave tank	Simulator
$\overline{\theta}$	8.01E−2 rad	5.02E−2 rad
$\sigma(\theta)$	7.47E−3 rad	3.67E−3 rad
$\overline{\phi}$	4.18E−3 rad	6.32E−8 rad
$\overline{\psi}$	2.85E−2 rad	−9.36E−5 rad
Line tension 1	2.43E6 N	2.50E6 N
Line tension 2	4.86E5 N	4.70E5 N
Line tension 3	1.31E5 N	4.71E5 N

The bathymetry and a Traffic Separation Scheme (International Maritime Organization (IMO), 2013) on the way of the route are taken into account, therefore the constraint is maintaining the towing in safe, open waters. As stated above, unsafe is considered either when the *VolturnUS* reaches a position where there is less than 40 m depth, or when the vessel is too close to the Isles of Scilly's Traffic Separation Scheme. The forbidden zone designated for the latter is a rectangle with the following boundaries: the longitudes of the extremities are 6.897° West and 5.83°, and the latitudes of the extremities are 50.339 ° North and 49.58° North.

For the single-objective optimisations, the objective is a weighted value of the preceding objectives. The different objective weights have been chosen using the order of magnitudes of the values obtained for each objective in multi-objective optimisations. The priority is given to the carbon emissions, then to the duration of the transportation, and finally to the tension of the towing line. Two sets of weights are used and the associated optimisations are named O99 and O90. For clarity, the weights are given in Table 8.

4. Results

4.1. Comparison with experiments in wave tank

The mean values of tensions in the different lines and of the attitude angles are presented in Tables 9 and 10 for the two different sea states, along with the standard deviation of the pitch angle. Tension in line n is named *line tension n*, for $n \in \{1, 2, 3\}$.

4.2. Optimisation

The results are represented in three different planes from the objective space in Figs. 10–12. The solutions obtained by single-objective optimisations are represented in red. The results of the multi-objective optimisations with tidal currents taken into account are shown in

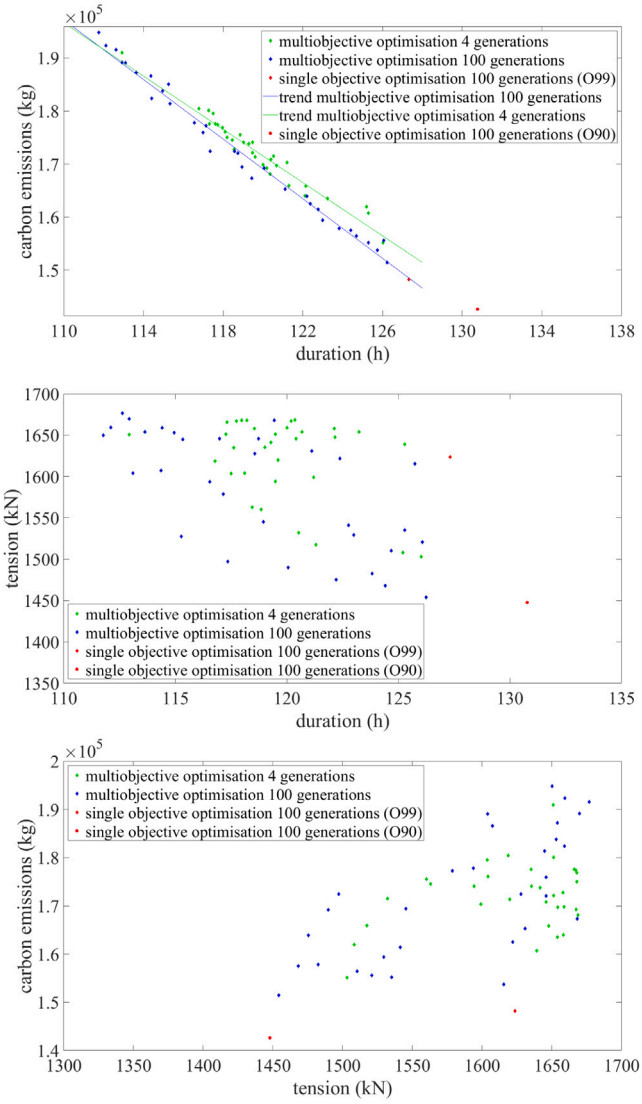

Fig. 10. Representation of the optimised solutions for the year 2020 in three different planes from objective space.

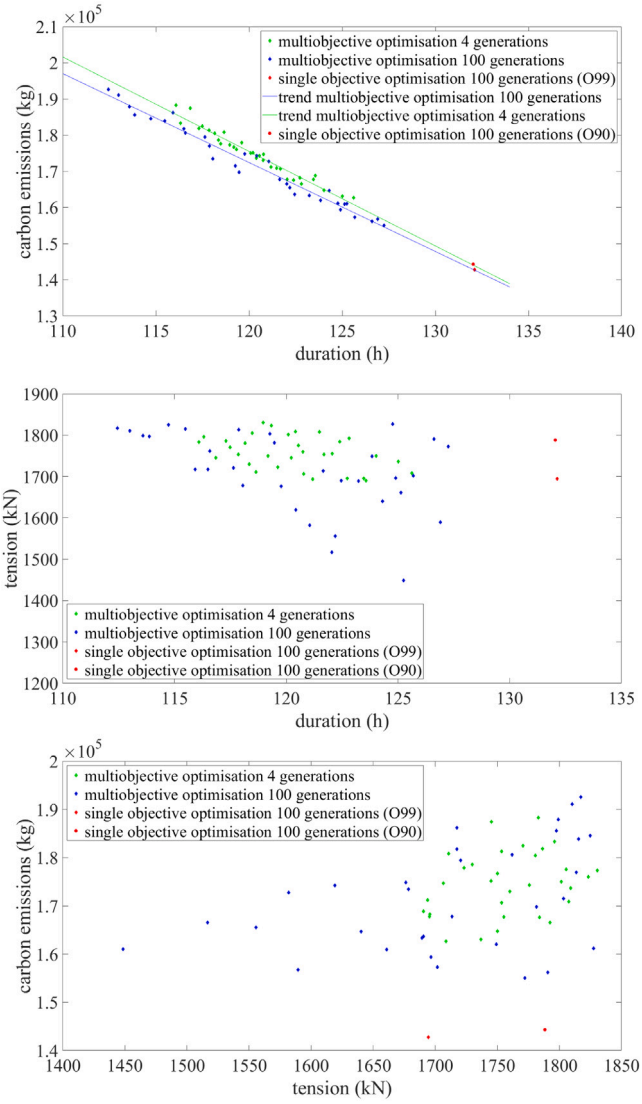

Fig. 11. Representation of the optimised solutions for the year 2021 in three different planes from objective space.

Figs. 13–15. Some optimised routes have been plotted on Figs. 16 and 17. The routes obtained by multi-objective optimisations are represented with dark green, red and blue. In dark green is the route with lowest carbon emissions, in blue the route with lowest tension in the towing line, and in red the fastest. Light green is the route calculated by O99 and in black is the route calculated by O90.

The amplitudes of the values obtained by multi-objective optimisation are presented in Table 11.

The wind during the transportation is shown in Figs. 18–35.

5. Discussion

5.1. Comparison with experiments in wave tank

The experiment, according to its specifications (Tosdevin et al., 2023), is symmetric around the x-axis and the tension in lines 2 and 3 should be the same. As well, the ideal values of the mean yaw angle and mean roll angle should be 0.

The tension in line 3 is lesser than in line 2 in the wave tank results, the relative differences being 3.1 for the first sea state and 3.7 for the second. The weaker tension in line 3 is the primary cause of any other asymmetry found in the results of the experiments performed in the wave tank. No major difference between tension in line 2 and 3 is observed in the ship simulator.

The absolute value of the mean yaw angle is larger in the wave tank results than in the ship simulator, with relative differences of 218 and 304. The absolute value of the mean roll angle is larger in the wave tank than in the ship simulator as well; the relative differences are 2.0×10^6 and 6.6×10^4.

The ability to reproduce an ideal experiment is clearly easier in the simulator than it is in a wave tank. The lower tension in line 3 in the wave tank is the cause of misalignment and of the non-zero roll angle in their results.

The observed mean pitch angle from the wave tank and the ship simulator is similar for both sea states, which is coherent with the fact that the thrust is identical. However, the value observed in the wave tank is larger with a difference of $3{\times}10^{-2}$ rad.

The amplitudes of pitch oscillations of the *VolturnUS* are small. In the ship simulator, the amplitudes of pitch motion are relatively similar compared to the wave tank, where they are multiplied by 3.6 between

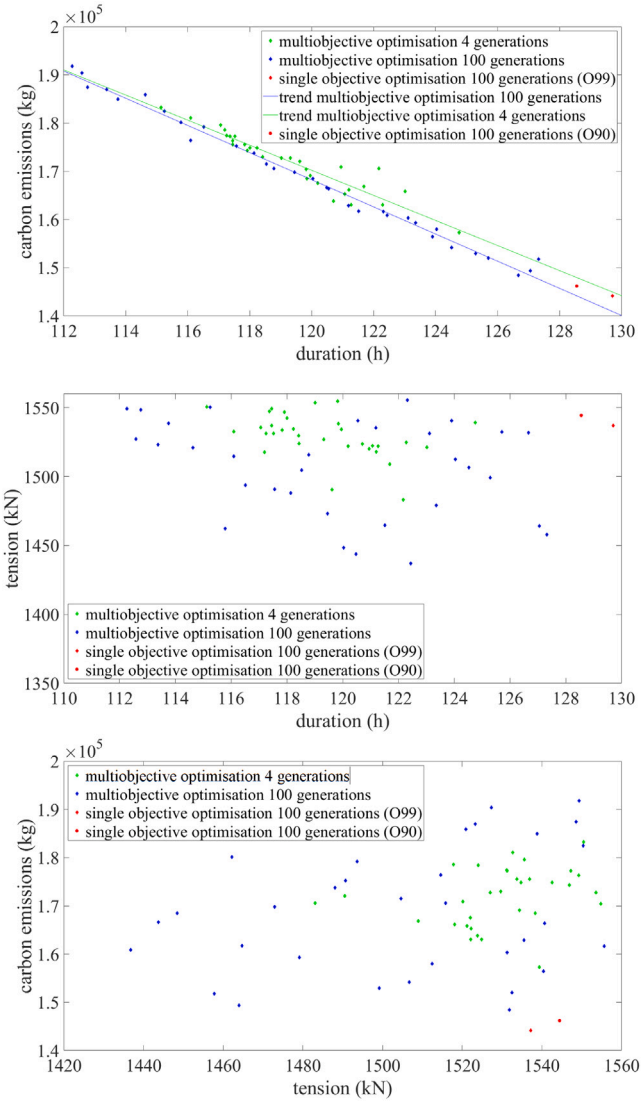

Fig. 12. Representation of the optimised solutions for the year 2022 in three different planes from objective space.

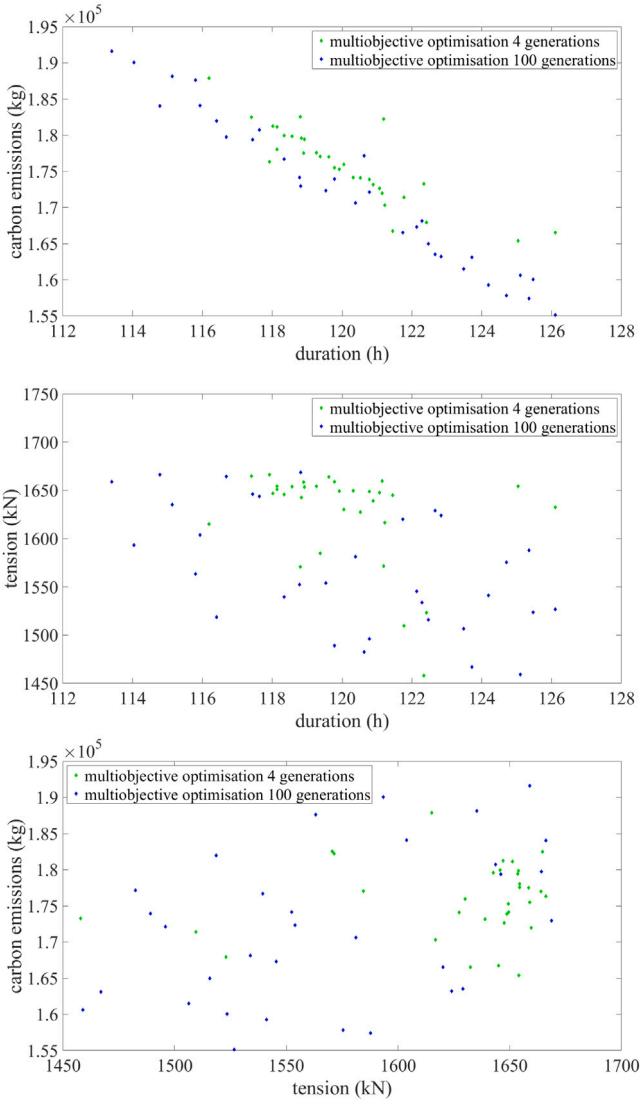

Fig. 13. Representation of the optimised solutions for the year 2020 in three different planes from objective space when tidal currents are taken into account.

the first and second sea state. These discrepancies could be explained mainly by some differences between the experiment in the wave tank and in the ship simulator. Nonetheless, the order of magnitudes are similar, suggesting that the simulator is therefore able to reasonably reproduce the motions of a vessel.

5.2. Optimisations

The results are presented in three different planes of objective space.

In the *duration – carbon emissions* plane, see Figs. 10–15, top graphic, the results of the multi-objective optimisations are spread along straight lines. This suggests that the minimised *duration* and *carbon emissions* oppose each other. For the three different days considered, the trend is slightly better after 100 generations than after four generations. The amplitude of values is larger for the solutions after 100 generations.

In the two other plane representations, the amplitude of values is larger for the solutions after 100 generations. The results of the multi-objective optimisation are spread in finite areas of the planes and their distribution does not follow any trend. This suggests that the *tension* in the towing line can be minimised at the same time as minimising the *carbon emissions* or the *duration*.

In multi-objective optimisation, when the tidal currents are not taken into account, the amplitude of values for the *carbon emissions* is about 20% for the three different days evaluated. The amplitude of values for the *duration* is between 11% and 12% for all years. The amplitudes of values of the *tensions* vary more among the days. Minimising the *carbon emissions* is therefore an objective that can lead to substantial results as shown by the magnitude of its amplitude.

The single-objective optimisations results appear to respond to the same trends as multi-objective results. Except for simulation O90 for the day in the year 2020, the results for the *tension* in the towing line given by the single-objective optimisations are equivalent to the results given by multi-objective optimisations (see Figs. 10–15, middle graphic). The results for the *duration* are always larger. The *carbon emissions* is smaller with single-objective optimisations. Nevertheless, the relative difference with respect to the multi-objective optimisation is negligible (see Table 12) and, therefore, single-objective optimisations have not been furthered to consider tidal currents.

When the tidal currents are taken into account, the solutions do not show any noticeable differences for the *duration*, the *carbon emissions*,

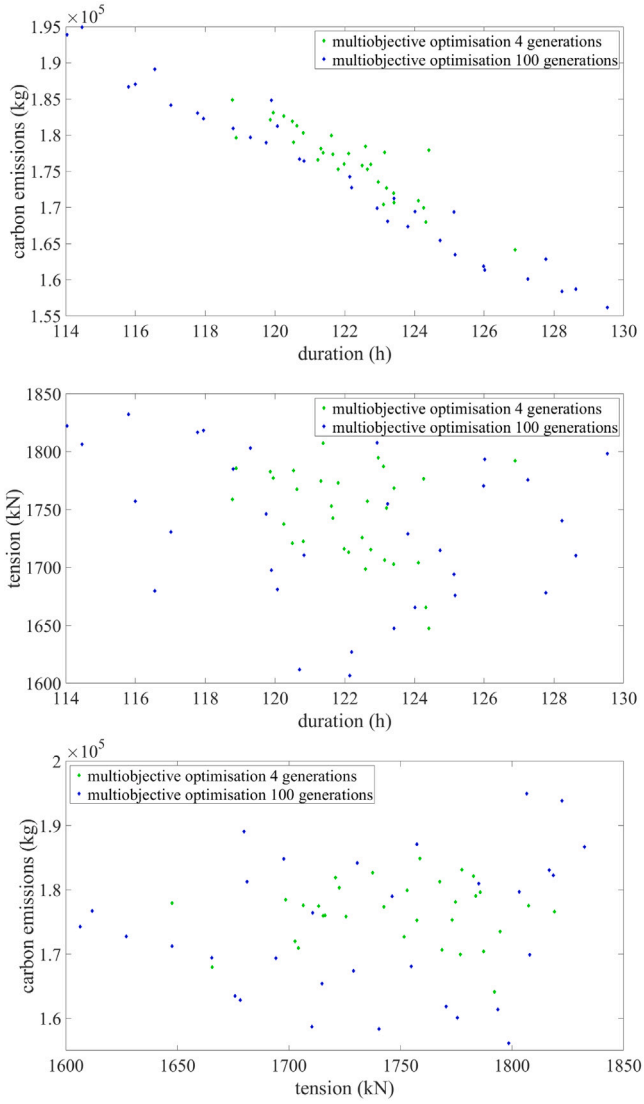

Fig. 14. Representation of the optimised solutions for the year 2021 in three different planes from objective space when tidal currents are taken into account.

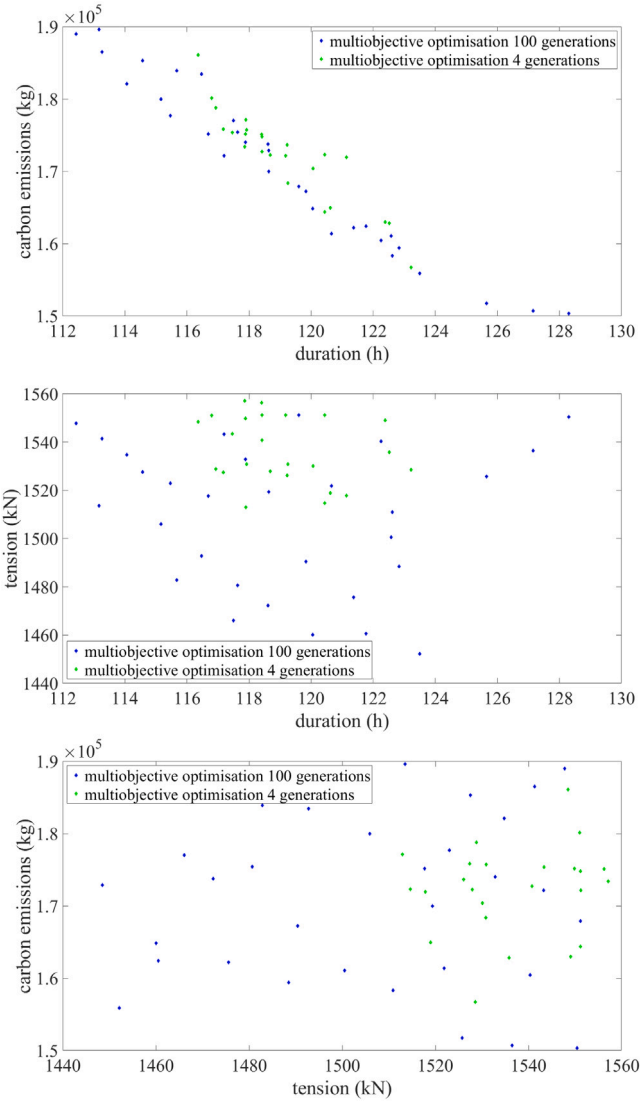

Fig. 15. Representation of the optimised solutions for the year 2022 in three different planes from objective space when tidal currents are taken into account.

and the *tension* with respect to the results when the currents are not taken into account. On the other hand, the resulting routes are different, since the positions are not part of the optimisation. The speed of currents was up to 2.24 m/s in the route of 2020, 1.53 m/s in 2021, and 2.17 m/s in 2022, which is in the same order of magnitude of the speed of the vessel. Note that the cyclic nature of tidal currents may be producing these observed results. Assuming from the above that the absence of tidal currents does not affect the *carbon emissions*, *duration*, and *tension* in towing line, it could then be disregarded to reduce the computation time. Nevertheless, such an assumption could not be used to determine optimal routes.

It is worth commenting that traditional quality indicators which compare the Pareto front approximations produced with the Pareto front have not been used, since the true Pareto front is unknown.

6. Conclusions

This paper has presented a new ship simulator, and demonstrates a methodology for using it to optimise oceanic routes for the wet towing of a floating offshore wind turbine. The simulator calculates in real time forces acting on the modelled objects using algebraic equations, which require detailed coefficients to accurately capture objects' behaviour. This has the advantage of enabling rapid experimentation and data generation in a safe, virtual environment, with the drawback of requiring quality input data —coefficients— capable of fully describing the simulated objects across the range of conditions they are subject to. This input data can be obtained from either practical experimentation or higher fidelity numerical models, such as CFD, and ideally needs to be verified and validated. Assumptions can be made in the absence of appropriate data as a starting point, but this may naturally impact the accuracy of results.

For this work, a model of the *VolturnUS* semi-submersible platform supporting the IEA 15 MW reference turbine was developed for the ship simulator. The platform model uses approximate data for viscous resistance and is in a fully ballasted configuration (i.e. has a draught of nearly 20 m) for all cases. The latter was done so that the implementation could be verified against experimental wave tank data for the case of a moored platform under wave excitation. This comparison does not fully validate the ship simulator's accuracy, but the similar orders of magnitude of the motion observed when comparing behaviour under moored conditions provide initial verification that the hydrostatics of

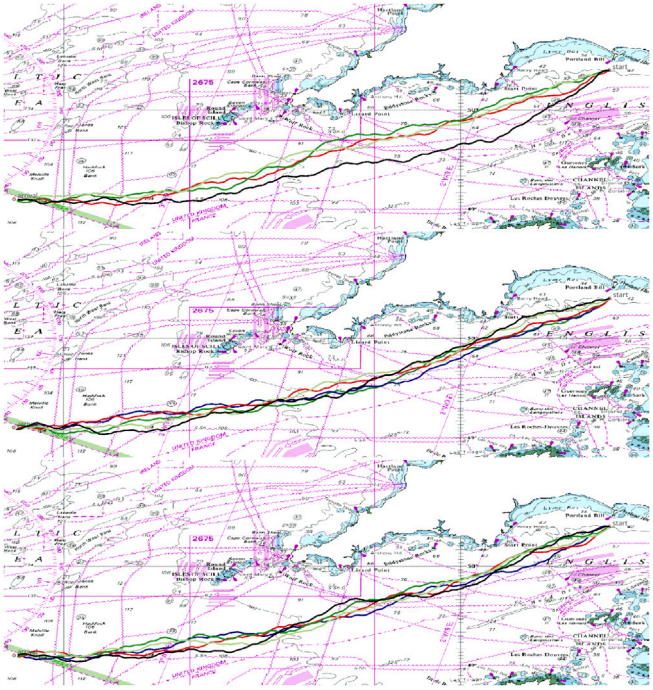

Fig. 16. Optimised routes when tidal currents are not taken into account.

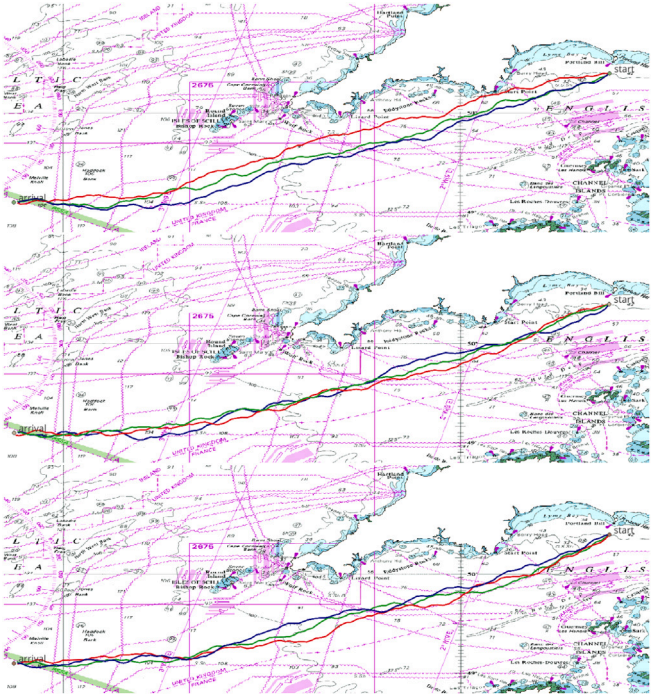

Fig. 17. Optimised routes when tidal currents are taken into account.

the digital model have been implemented reliably. Further comparisons against towing data and improved viscous drag data are required to fully validate the model, particularly for the more realistic case of a fully deballasted platform under tow. This is an avenue for future work as the experimental or numerical data required for implementing this configuration within the ship simulator, as well as for validation of comparisons, are not yet available.

Despite this limitation, the presented methodology shows the potential advantage for using such simulators to reduce uncertainty in offshore operations such as wet towing. Many experimental runs were conducted for the presented case of a single vessel towing the platform in oceanic conditions. Predicted towing speeds of up to 3.21 m/s — 6.25 knots— are realistic for this scenario. Data from the runs was used to generate an empirical model relating vessel engine power, towline tension, and surge velocity to true wind speed, wind angle, and ship's engine order. This enabled the use of both single-objective, `Mixed-VariableGA` algorithm, and multi-objective, NSGA-II algorithm, optimisations for identifying navigation routes that minimised carbon emissions, journey duration, and towline tensions for the oceanic portion of transits between the Bill of Portland and a potential wind farm site in the Celtic Sea. This was done using hindcast metocean data from Augusts of 2020, 2021, and 2022. The results of the single-objective optimisations show a similar trend to the multi-objective optimisation and are therefore considered of limited interest. The role of tidal currents has also been evaluated, since the currents are of similar magnitude to the vessel speed and, therefore, cannot be neglected for a correct routing. Nonetheless, similar values for the *carbon emissions*, *duration* of the voyage and *tension* in the towing line between current and non-current cases indicate that tidal currents could be neglected for the sole purpose of evaluating oceanic routes using these quantities.

The methodology shown in this work could easily be expanded to other towing configurations —e.g. nearshore operations involving trailing tugs – or other parameters of interest – such as vessel fuel burn. This would facilitate rapid study and optimisation of operations that are currently introducing significant uncertainty for wind farm developers. This endeavour would benefit from several further advancements to

Table 11
Relative amplitudes of objectives, and time amplitudes for arrival.

Objective	Year	Currents	Interval
Carbon emissions	2020	No	22.26%
		Yes	19.05%
	2021	No	19.49%
		Yes	19.90%
	2022	No	22.62%
		Yes	20.73%
Duration	2020	No	11.46%
		Yes	10.07%
	2021	No	11.63%
		Yes	11.97%
	2022	No	11.82%
		Yes	12.37%
Tension in towing line	2020	No	13.29%
		Yes	12.56%
	2021	No	20.73%
		Yes	12.33%
	2022	No	7.64%
		Yes	6.62%
Arrival times	2020	No	22 h
		Yes	17 h
	2021	No	23 h
		Yes	18 h
	2022	No	21 h
		Yes	17 h

Table 12
Proportion of the objective in the cost function for single-objective optimisation and relative improvement for the carbon emissions.

Objective	Year	O99	O90
Carbon emissions	2020	0.9861	0.8753
	2021	0.9850	0.8670
	2022	0.9859	0.8766
Duration	2020	8.5E−3	8.03E−2
	2021	9.1E−3	7.93E−2
	2022	8.9E−3	7.71E−2
Improvement compared	2020	2.11%	5.82%
To the greenest solution	2021	7.95%	6.94%
From multi-objective optimisation	2022	2.89%	1.51%

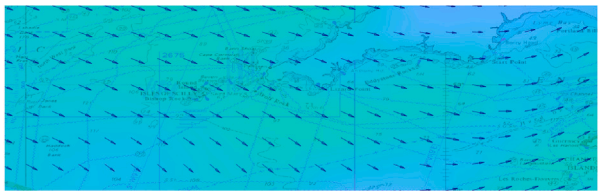

Fig. 18. Wind at 9 am on 1/8/2020.

improve on the present approach. Chief among these is the development of an improved model of the floating wind turbine itself, with the turbine more appropriately ballasted for towing and with accurate and validated coefficients for hydrodynamic factors. Inclusion of the initial nearshore portion of the tow, optimisation for different tow configurations, optimisation to find the best tow configuration, and optimisation within the context of the scheduling of port operations, equipment utilisation, and overall installation timescales, are also all avenues for future exploration.

CRediT authorship contribution statement

Frédéric Le Pivert: Conceptualisation, Data Curation, Formal analysis, Investigation, Software, Methodology, Visualisation, Validation, writing – original draft, writing – review and editing. **Adán López-Santander:** Conceptualisation, Funding acquisition, investigation, supervision, methodology, validation, writing – review and editing. **Matthew J. Craven:** Software, Methodology, validation, writing – review and editing. **Adam Roberts:** Writing – review and editing.

Declaration of competing interest

The authors declare the following financial interests/personal relationships which may be considered as potential competing interests: Adan Lopez-Santander reports financial support was provided by the European Regional Development Fund. If there are other authors, they declare that they have no known competing financial interests or personal relationships that could have appeared to influence the work reported in this paper.

Data availability

Data will be made available on request.

Acknowledgements

The authors acknowledge Anna Holcombe, Dr Emma Edwards, Tom Tosdevin and Dr Martyn Hann for their help and data sharing about the *VolturnUS*. The authors acknowledge Karsten Haegg, Thorvald Grindstad and Daniel Broberg from Kongsberg Digital for providing training and helping to use the simulator.

Appendix. Wind data

See Figs. 18–35.

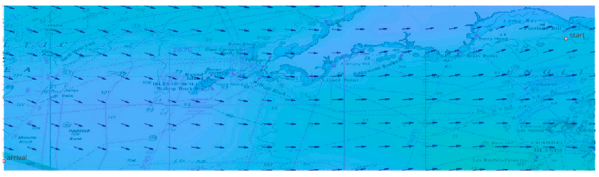

Fig. 19. Wind at 9 am on 2/8/2020.

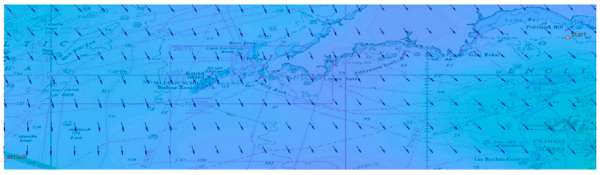

Fig. 20. Wind at 9 am on 3/8/2020.

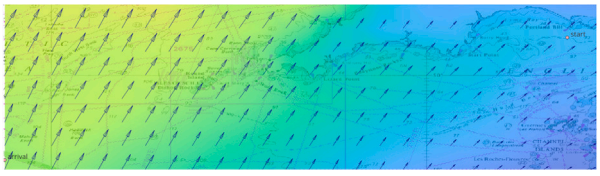

Fig. 21. Wind at 9 am on 4/8/2020.

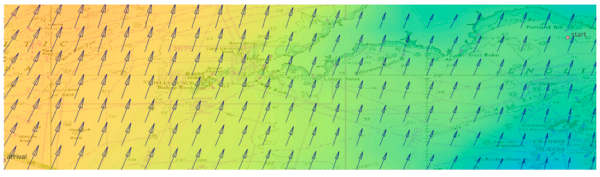

Fig. 22. Wind at 9 am on 5/8/2020.

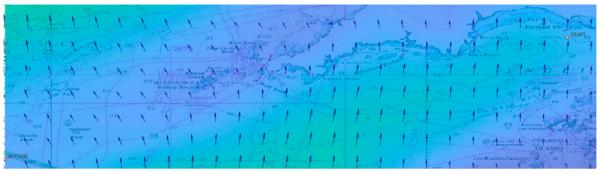

Fig. 23. Wind at 9 am on 6/8/2020.

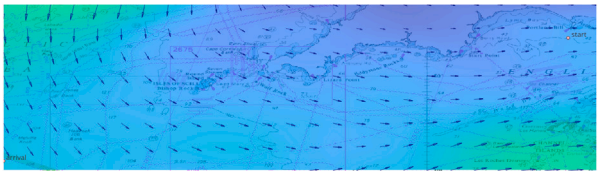

Fig. 24. Wind at 9 am on 1/8/2021.

Fig. 25. Wind at 9 am on 2/8/2021.

Fig. 26. Wind at 9 am on 3/8/2021.

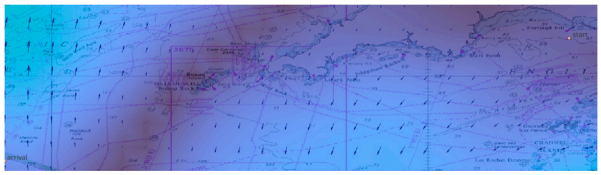

Fig. 27. Wind at 9 am on 4/8/2021.

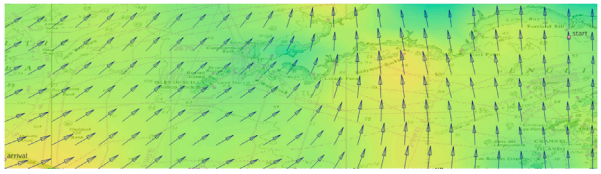

Fig. 28. Wind at 9 am on 5/8/2021.

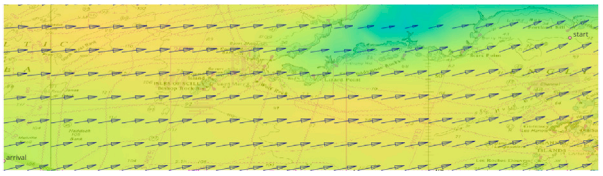

Fig. 29. Wind at 9 am on 6/8/2021.

Fig. 30. Wind at 9 am on 1/8/2022.

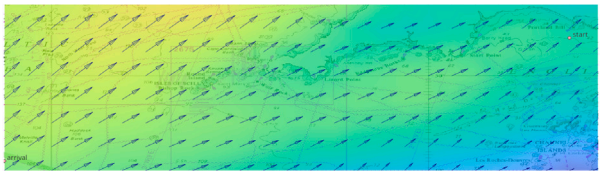

Fig. 31. Wind at 9 am on 2/8/2022.

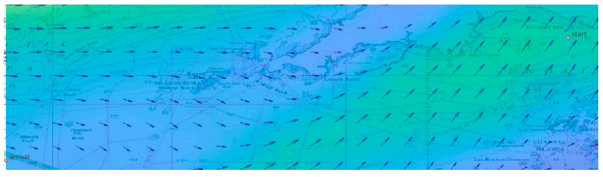

Fig. 32. Wind at 9 am on 3/8/2022.

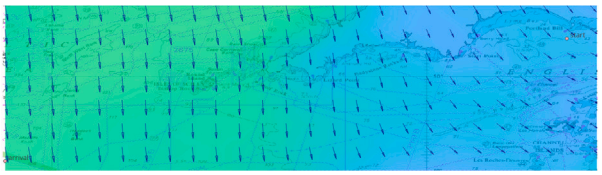

Fig. 33. Wind at 9 am on 4/8/2022.

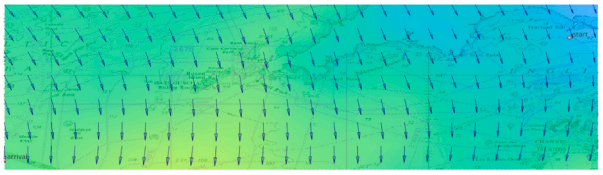

Fig. 34. Wind at 9 am on 5/8/2022.

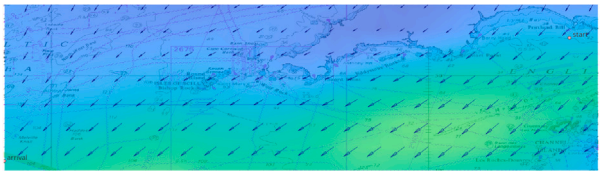

Fig. 35. Wind at 9 am on 6/8/2022.

References

Allen, C., Viselli, A., Dagher, H., Goupee, A., Gaertner, E., Abbas, N., Hall, M., Barter, G., 2020. Definition of the UMaine VolturnUS-S Reference Platform Developed for the IEA Wind 15-Megawatt Offshore Reference Wind Turbine. Technical Report, International Energy Agency, URL: https://www.nrel.gov/docs/fy20osti/76773.pdf.

Amin, I., Oterkus, S., Ali, M.E., Shawky, H., Oterkus, E., 2021. Experimental investigation on a towing assessment for a floating desalination plant for Egypt. Ocean Eng. 238, 109746.

Blank, J., Deb, K., 2020. Pymoo: Multi-objective optimization in python. IEEE Access 8, 89497–89509.

Castro-Santos, L., Diaz-Casas, V., 2014. Life-cycle cost analysis of floating offshore wind farms. Renew. Energy 66, 41–48.

Chauveau, E., Jégou, P., Prcovic, N., 2017. Weather routing optimization: A new shortest path algorithm. In: 2017 IEEE 29th International Conference on Tools with Artificial Intelligence. ICTAI, pp. 687–694. http://dx.doi.org/10.1109/ICTAI.2017.00110.

Dagher, H., Viselli, A., Goupee, A., Kimball, R., Allen, C., 2017. The VolturnUS 1: 8 Floating Wind Turbine: Design, Construction, Deployment, Testing, Retrieval, and Inspection of the First Grid-Connected Offshore Wind Turbine in US. Technical Report, Univ. of Maine, Orono, ME (United States).

Deb, K., Pratap, A., Agarwal, S., Meyarivan, T., 2002. A fast and elitist multiobjective genetic algorithm: NSGA-II. IEEE Trans. Evol. Comput. 6 (2), 182–197.

DNV-GL DET NORSKE VERITAS, 2017. Maritime simulator systems. Standard: DNVGL-ST-0033.

Du, W., Li, Y., Zhang, G., Wang, C., Chen, P., Qiao, J., 2021. Estimation of ship routes considering weather and constraints. Ocean Eng. 228, 108695.

Du, W., Li, Y., Zhang, G., Wang, C., Zhu, B., Qiao, J., 2022. Energy saving method for ship weather routing optimization. Ocean Eng. 258, 111771.

E.U. Copernicus Marine Service Information, 2024. Atlantic - European North West Shelf - Ocean Physics Analysis and Forecast [dataset]. DOI: https://doi.org/10.48670/moi-00054.

European Centre for Medium-Range Weather Forecasts (ECMWF), 2005. Eccodes.

Fabbri, T., Vicen-Bueno, R., 2019. Weather-routing system based on METOC navigation risk assessment. J. Mar. Sci. Eng. 7 (5), 127.

Gaertner, E., Rinker, J., Sethuraman, L., Zahle, F., Anderson, B., Barter, G., Abbas, N., Meng, F., Bortolotti, P., Skrzypinski, W., Scott, G., Feil, R., Bredmose, H., Dykes, K., Sheilds, M., Allen, C., Viselli, A., 2020. Definition of the IEA 15-Megawatt Offshore Reference Wind Turbine. Technical Report, International Energy Agency, URL: https://www.nrel.gov/docs/fy20osti/75698.pdf.

Gai, W.-M., Deng, Y.-F., Jiang, Z.-A., Li, J., Du, Y., 2017. Multi-objective evacuation routing optimization for toxic cloud releases. Reliab. Eng. Syst. Saf. 159, 58–68.

Gershanik, V., 2011. Weather routing optimisation–challenges and rewards. J. Mar. Eng. Technol. 10 (3), 29–40.

Grifoll, M., Borén, C., Castells-Sanabra, M., 2022. A comprehensive ship weather routing system using CMEMS products and A* algorithm. Ocean Eng. 255, 111427. http://dx.doi.org/10.1016/j.oceaneng.2022.111427, URL: https://www.sciencedirect.com/science/article/pii/S0029801822008095.

Hersbach, H., Bell, B., Berrisford, P., Biavati, G., Horanyi, A., Muñoz Sabater, J., Nicolas, J., Peubey, C., Radu, R., Rozum, I., Schepers, D., Simmons, A., Soci, C., Dee, D., Thepaut, J.-N., 2023. ERA5 hourly data on single levels from 1940 to present..

Holcombe, A., Edwards, E., Tosdevin, T., Greaves, D., Hann, M., 2023. A comparative study of potential-flow-based numerical models to experimental tests of a semi-submersible floating wind turbine platform. In: ISOPE International Ocean and Polar Engineering Conference. ISOPE, pp. ISOPE–I.

International Maritime Organization (IMO), 2013. Ships Routeing, 2013 Edition IMO Publishing, London.

James, R.W., 1957. Application of Wave Forecasts to Marine Navigation. Ph.D. Thesis, New York University.

Jiao, G., Liu, Q., Mao, L., Guo, X., 2017. Pipe routing for aero-engine using modified MOEA/d. In: 2017 10th International Symposium on Computational Intelligence and Design. ISCID, Vol. 2, IEEE, pp. 59–63.

Kaldellis, J., Apostolou, D., 2017. Life cycle energy and carbon footprint of offshore wind energy. comparison with onshore counterpart. Renew. Energy 108, 72–84.

Kim, B., Kim, T.-W., 2017a. Weather routing for offshore transportation using genetic algorithm. Appl. Ocean Res. 63, 262–275. http://dx.doi.org/10.1016/j.apor.2017.01.015, URL: https://www.sciencedirect.com/science/article/pii/S0141118716302991.

Kim, B., Kim, T.-W., 2017b. Weather routing for offshore transportation using genetic algorithm. Appl. Ocean Res. 63, 262–275.

Konak, A., Coit, D.W., Smith, A.E., 2006. Multi-objective optimization using genetic algorithms: A tutorial. Reliab. Eng. Syst. Saf. 91 (9), 992–1007.

Krata, P., Szlapczynska, J., 2018. Ship weather routing optimization with dynamic constraints based on reliable synchronous roll prediction. Ocean Eng. 150, 124–137.

Kuhlemann, S., Tierney, K., 2020. A genetic algorithm for finding realistic sea routes considering the weather. J. Heuristics 26 (6), 801–825. http://dx.doi.org/10.1007/s10732-020-09449-7.

Kuroda, M., Sugimoto, Y., 2022. Evaluation of ship performance in terms of shipping route and weather condition. Ocean Eng. 254, 111335.

Le, C., Ren, J., Wang, K., Zhang, P., Ding, H., 2021. Towing performance of the submerged floating offshore wind turbine under different wave conditions. J. Mar. Sci. Eng. 9 (6), 633.

Leimeister, M., Kolios, A., Collu, M., 2018. Critical review of floating support structures for offshore wind farm deployment. In: Journal of Physics: Conference Series. Vol. 1104, IOP Publishing, 012007.

Lin, Y.-H., Fang, M.-C., Yeung, R.W., 2013. The optimization of ship weather-routing algorithm based on the composite influence of multi-dynamic elements. Appl. Ocean Res. 43, 184–194. http://dx.doi.org/10.1016/j.apor.2013.07.010, URL: https://www.sciencedirect.com/science/article/pii/S0141118713000679.

Liu, B., Yu, J., 2022. Dynamic response of SPAR-type floating offshore wind turbine under wave group scenarios. Energies 15 (13), 4870.

Martins, E.Q.V., 1984. On a multicriteria shortest path problem. European J. Oper. Res. 16 (2), 236–245.

Myland, T., Adam, F., Dahlias, F., Großmann, J., 2014. Towing tests with the GICON®-TLP for wind turbines. In: The Twenty-Fourth International Ocean and Polar Engineering Conference. OnePetro.

OceanWise, 2023. Marine themes vector. URL: https://digimap.edina.ac.uk. Scale 1:25000.

Park, S.H., Lee, S.J., Lee, S., 2021. Experimental investigation of towing-and course-stability of a FPSO towed by a tug-boat with lateral motion. Int. J. Nav. Archit. Ocean Eng. 13, 12–23.

Ransley, E., Brown, S., Edwards, E., Tosdevin, T., Monk, K., Reynolds, A., Greaves, D., Hann, M., 2022. Hydrodynamic Response of a Floating Offshore Wind Turbine (1st FOWT Comparative Study Dataset). Technical Report, PEARL Research Repository.

Shao, W., Zhou, P., Thong, S.K., 2012. Development of a novel forward dynamic programming method for weather routing. J. Mar. Sci. Technol. 17 (2), 239–251. http://dx.doi.org/10.1007/s00773-011-0152-z.

Solstad, 2010. Solstad. URL: https://www.solstad.com.

Solstad Offshore, 2023. AHTS normand ranger.

Sykes, V., Collu, M., Coraddu, A., 2023. A review and analysis of the uncertainty within cost models for floating offshore wind farms. Renew. Sustain. Energy Rev. 186, 113634.

Szlapczynska, J., Smierzchalski, R., 2007. Adopted isochrone method improving ship safety in weather routing with evolutionary approach. Int. J. Reliab. Qual. Saf. Eng. 14 (06), 635–645. http://dx.doi.org/10.1142/s0218539307002842, URL: https://www.worldscientific.com/doi/abs/10.1142/S0218539307002842.

Szlapczynska, J., Szlapczynski, R., 2019. Preference-based evolutionary multi-objective optimization in ship weather routing. Appl. Soft Comput. 84, 105742.

The Crown Estate, 2023. Information memorandum - celtic sea floating offshore wind - leasing round 5. URL: https://downloads.ctfassets.net/nv65su7t80y5/5zR4gHuqxjMG9NOK1LI2Av/643bfa91696be32408e5e2646c16bbba/Information_Memorandum.pdf.

Tosdevin, T., Edwards, E., Holcombe, A., Brown, S., Ransley, E., Hann, M., Greaves, D., 2023. On the use of response conditioned focused wave and wind events for the prediction of design loads. In: International Conference on Offshore Mechanics and Arctic Engineering. Vol. 87578, American Society of Mechanical Engineers.

Ulstein, 2010. Ulstein. URL: https://ulstein.com.

Vettor, R., Bergamini, G., Guedes Soares, C., 2021. A comprehensive approach to account for weather uncertainties in ship route optimization. J. Mar. Sci. Eng. 9 (12), 1434.

Vettor, R., Guedes Soares, C., 2022. Reflecting the uncertainties of ensemble weather forecasts on the predictions of ship fuel consumption. Ocean Eng. 250, 111009.

Vettor, R., Szlapczynska, J., Szlapczynski, R., Tycholiz, W., Guedes Soares, C., 2020. Towards improving optimised ship weather routing. Pol. Marit. Res. 27 (1), 60–69.

Virtanen, P., Gommers, R., Oliphant, T.E., Haberland, M., Reddy, T., Cournapeau, D., Burovski, E., Peterson, P., Weckesser, W., Bright, J., van der Walt, S.J., Brett, M., Wilson, J., Millman, K.J., Mayorov, N., Nelson, A.R.J., Jones, E., Kern, R., Larson, E., Carey, C.J., Polat, İ., Feng, Y., Moore, E.W., VanderPlas, J., Laxalde, D., Perktold, J., Cimrman, R., Henriksen, I., Quintero, E.A., Harris, C.R., Archibald, A.M., Ribeiro, A.H., Pedregosa, F., van Mulbregt, P., SciPy 1.0 Contributors, 2020. SciPy 1.0: Fundamental Algorithms for Scientific Computing in Python. Nature Methods 17, 261–272. http://dx.doi.org/10.1038/s41592-019-0686-2.

Walther, L., Rizvanolli, A., Wendebourg, M., Jahn, C., 2016. Modeling and optimization algorithms in ship weather routing. Int. J. e-Navig. Marit. Econ. 4, 31–45. http://dx.doi.org/10.1016/j.enavi.2016.06.004, URL: https://www.sciencedirect.com/science/article/pii/S2405535216300043.

WAMIT, i., 2011. WAMIT, user manual.

Wang, H., Mao, W., Eriksson, L., 2017. Benchmark study of five optimization algorithms for weather routing. In: International Conference on Offshore Mechanics and Arctic Engineering. Vol. 57748, American Society of Mechanical Engineers, V07BT06A023.

Zaccone, R., Figari, M., Martelli, M., 2018. An optimization tool for ship route planning in real weather scenarios. In: The 28th International Ocean and Polar Engineering Conference. OnePetro, pp. 738–744.

Zhu, H., Hu, C., 2021. A unified seakeeping and maneuvering analysis of multiple linked towing system with triangular bodies. Ocean Eng. 222, 108577.